


## Article

# Experimental Study on the Influence of Moisture and Clay Content on Stress Wave Attenuation Characteristics of Filled Joints

Sheng Li, Ziming Xiong , Pengxian Fan \* and Kaidi Xie

State Key Laboratory for Disaster Prevention &amp; Mitigation of Explosion &amp; Impact, Army Engineering University of PLA, Nanjing 210007, China

\* Correspondence: fan-px@139.com

**Abstract:** Artificial filled joints made of sand–clay mixtures with different clay weight fractions and saturations have different wave attenuation capacities. In this paper, the high amplitude impact test of sand–clay mixtures was carried out by using split Hopkinson pressure bar (SHPB) equipment. The results showed that with the increase of clay weight fraction, the particle crushing decreased continuously, while the wave attenuation coefficient decreased first and then increased. When the weight fraction of clay was 50%, the wave attenuation coefficient reached the minimum among the tested working conditions, and the ratio of transmitted energy to incident energy reached the maximum. With the increase of saturation, the particle crushing decreased first and then increased, while the wave attenuation coefficient increased first and then decreased. When the saturation was 25%, the wave attenuation coefficient reached the maximum, and the proportion of transmitted energy to incident energy reached the minimum. Because of the lubrication of water reduced the friction between particle, the specimen more prone to deformation and particle crushing reduced. As the saturation increased, this effect gradually decreased. In the case of the wave absorbing layer of protective works, special attention should be paid to the adverse effects caused by groundwater.

**Keywords:** rock joint; stress wave; moisture content; mixing ratio; energy distribution



**Citation:** Li, S.; Xiong, Z.; Fan, P.; Xie, K. Experimental Study on the Influence of Moisture and Clay Content on Stress Wave Attenuation Characteristics of Filled Joints. *Appl. Sci.* **2022**, *12*, 9140. <https://doi.org/10.3390/app12189140>

Academic Editor: Arcady Dyskin

Received: 29 August 2022

Accepted: 8 September 2022

Published: 12 September 2022

**Publisher's Note:** MDPI stays neutral with regard to jurisdictional claims in published maps and institutional affiliations.



**Copyright:** © 2022 by the authors. Licensee MDPI, Basel, Switzerland. This article is an open access article distributed under the terms and conditions of the Creative Commons Attribution (CC BY) license (<https://creativecommons.org/licenses/by/4.0/>).

## 1. Introduction

There are a lot of natural joints in the rock mass around strategic protection engineering, which are often filled with sand and clay. Such granular materials are usually weak and have a large difference in wave impedance from natural rocks [1]. Reflection and attenuation occurred in rock joints during stress wave propagation. At the same time, the infill squeezed each other and broke by friction. This process consumes a large amount of incident energy and effectively weakens the stress wave intensity [2]. The weakening effect was significantly different with different filling materials. Therefore, by discussing the seismic response of rock joints filled with different granular materials under a seismic wave, especially under high strain rate conditions, recommendations are provided for existing absorbing layer materials and further weaken the damage effect of ground penetrating weapons and nuclear blast effects on protective works [3].

Under high strain rate conditions, inertial force would be generated when the loading rate exceeded the quasi-stationary state region. At the macroscopic scale, this is manifested in the form of increased stiffness and strength; at the particle scale, changes in the forces between particles may lead to fragmentation of the particles, thus affecting the energy dissipation of wave propagation. The split Hopkinson pressure bar (SHPB) equipment was widely used in the high strain rate laboratory test. By using the modified Kolsky method [4], the sand or clay was confined in the rigid sleeve to limit its radial strain. This method has a good effect in an impact test. By using the shell theory, Chen et al. [5] proposed an alternative theoretical method to estimate the stress and deformation state of granular materials in passive constrained SHPB tests. Then, high strain rate impact tests were

carried out on calcareous sand with water content of 25% and 30% to verify the feasibility of the theoretical method. By using the modified Kolsky method, Wang et al. [6] carried out high strain rate impact tests on Stockton beach sand with different initial densities and saturations. Luo et al. [7] explored the effect of mass density on the compressive properties of dry sand, and pointed out that the dynamic stress–strain relationship of dry sand under constraint conditions was highly sensitive to the initial mass density. Meanwhile, Luo et al. [7] estimated the energy absorption characteristic of sand according to the area surrounded by the stress–strain curve, and found that the specific energy absorption range of dry sand was 5–25 J/g. Luo et al. [8] carried out high strain rate impact tests on sand with five water contents (mass ratios were 0%, 4.2%, 8.2%, 12.4% and 16.5%, respectively). The paper pointed out that the stress–strain behavior of partially saturated sand was strongly dependent on confining pressure, initial mass density and saturation degree. With the increase of saturation, the mechanical behavior of Eglin sand with mass density of 1.52 g/cm<sup>3</sup> was softening first and then becoming stiffer; but the lock-up phenomenon did not happen when the mass density of sand was 1.75 g/cm<sup>3</sup>. Barr et al. [9] studied the effect of water content on the compressibility and particle crushing of loose sand. The results were similar to those of Luo et al. [8]. When the moisture content reached 15.0%, the specimen was completely saturated and the particles were rarely crushed. Cola et al. [10] pointed out that under high strain rate impact, spherical particles were more difficult to be crushed and had a higher stress–strain relationship with the same compactness and lateral constraint. When the incident wave propagates through the rock joints, part of the wave will be reflected, part of the wave will be dissipated due to the friction and fragmentation of the particles inside the joints, and finally, the remaining part of the wave will continue to propagate. A lot of energy will be consumed in this process [11]. Meanwhile, some numerical methods have been developed based on the theory of stress wave propagation in jointed rock masses, such as finite difference, finite element and boundary element methods, etc. Lak et al. [12] derived a general Green's function solution to express the elastic wave propagation in rock blasting and a coupled finite difference-boundary element method cracks had been used to calculate the initiation and propagation due to an explosion in the rock [13]. Some researchers also pointed out two kinds of models: a thin-layer interface model and a zero-thickness model. According to the thin-layer inter-face model, the displacement at each side of the rock joints was continuous. However, there is a distinct jump in the displacement at the zero-thickness interface. Based on the above theory, many scholars have done a lot of research [14,15].

Fracture characteristics, loading conditions and material types are main factors influencing the seismic response of artificial filled joints under high strain rate impact. Under the action of a stress wave, both sand and clay show obvious viscoelastic behavior. The Kelvin model [16] was often used to describe the propagation of stress waves in clay. In natural rock joints, sand acted as a particle skeleton, and clay filled the space between the skeletons, which would reduce deformation of the skeleton under high-amplitude stress waves. Particularly, the mixing of clay, sand, water and air would significantly alter the joint characteristics. Luo et al. [17] made 'natural soil' by mixing dry clay and dry sand in different mass ratios. Then, the dynamic responses of different natural soils under dry and saturated conditions were compared. Wu et al. [18] conducted low-velocity impact tests on consolidated sand–clay mixtures with different clay weight fractions. Then, it was found that when the weight fraction of clay was 30%, the clay would completely fill the space between sand particles. While the joint stiffness reached the maximum, the transmission of seismic wave reached the maximum.

Through the above research, it can be found that the compressibility of clay, sand and water is obviously different. Different mixing ratio and saturation will significantly affect the wave transmission across the filled fracture. Meanwhile, the impact process is accompanied by obvious particle crushing and energy dissipation, but there are few reports related to these two perspectives. In this paper, the SHPB test system was used to carry out high amplitude impact tests on artificial filled joints with different clay contents and

moisture contents. The propagation law of the high amplitude stress wave was explored from the perspectives of energy distribution and particle crushing. The propagation law and stress wave attenuation characteristics in the different rock joints were studied, which enrich the research on the interaction between stress wave and filled fracture.

## 2. Test Method and Test Materials

### 2.1. Experimental Setup

In this paper, the experimental setup adopted the 50 mm split Hopkinson pressure bar system in the State Key Laboratory for Disaster Prevention & Mitigation of Explosion & Impact (Figure 1). The setup mainly consisted of 6 parts including plenum chamber, striker bar, incident bar, transmitted bar, buffer unit and signal collection device. Gas pressure in the plenum chamber was controlled by computer to drive the striker bar to the impact incident bar at different speeds. The incident compression waves with different amplitudes were formed in the incident bar to realize the different strain rate loading on the specimen. The materials of the incident bar, transmission bar and striker bar in the setup were 35CrMnSiA low alloy ultra-high strength steel with a density of  $7850 \text{ g/cm}^3$ , a longitude velocity of  $5440 \text{ m/s}$  and a Young's modulus of  $233 \text{ GPa}$ . Their lengths were  $3.0 \text{ m}$ ,  $2.5 \text{ m}$  and  $0.4 \text{ m}$ , respectively.

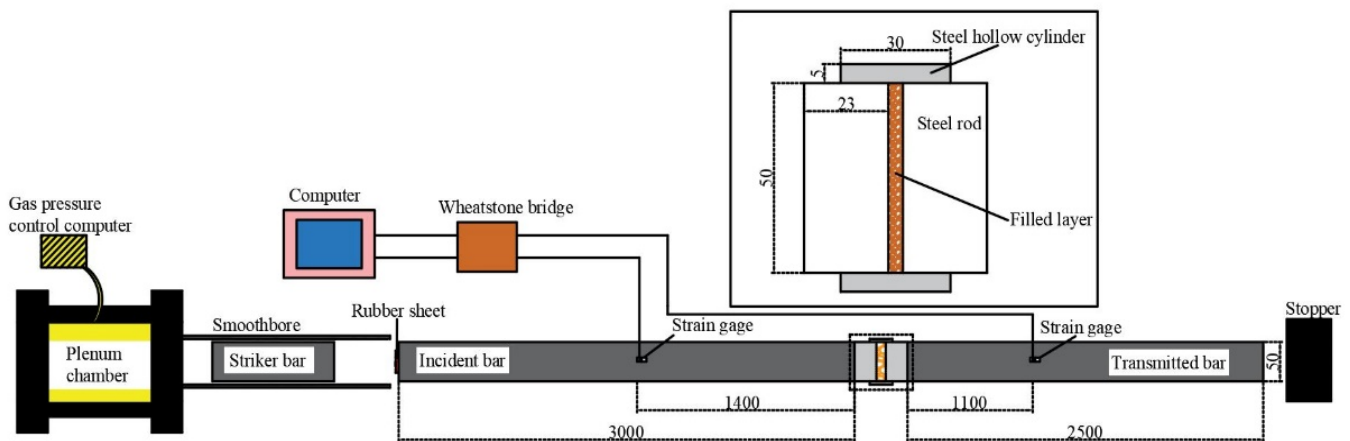
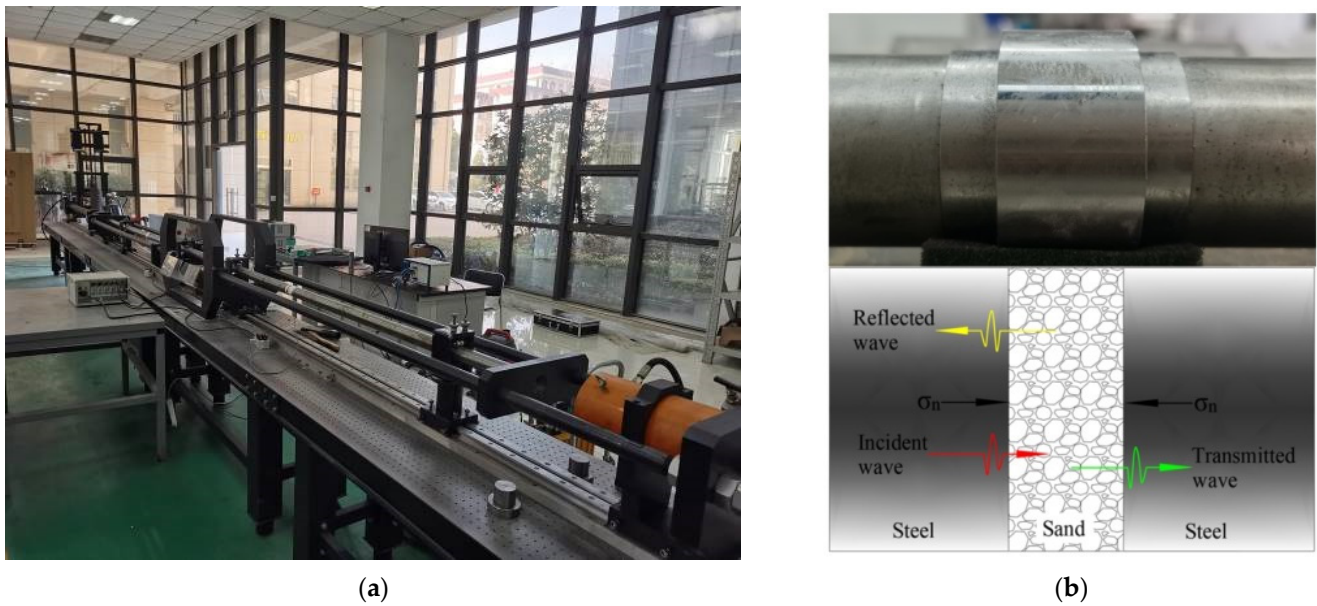


Figure 1. Split Hopkinson Pressure Bar.

In this paper, the method of Luo et al. [7] was used to construct artificially filled joints. 35CrMnSiA low alloy ultra-high strength steel was selected to make cushion blocks and sleeve (Figure 2). The device was carried out between the incident bar and the transmission bar after filling the sand into the cushion block and the sleeve. The sleeve had an inner diameter of  $50 \text{ mm}$ , an outer diameter of  $60 \text{ mm}$  and a length of  $30 \text{ mm}$ . The cushion block had a diameter of  $49.5 \text{ mm}$  and a length of  $23 \text{ mm}$ . Vaseline was applied between the cushion blocks and the sleeve to reduce the sliding friction force and increase seal performance.

To record the complete dynamic strain signal, the strain gauges were located in the points with a  $1400 \text{ mm}$  length from the end of the incident bar and a  $1100 \text{ mm}$  length from the start of the transmission bar, respectively. As the distance from the strain gauges to the end of the bars was long enough, the effect of the superposition of reflected waves on the data could be avoided. Data were recorded at  $1 \text{ MHz}$  digital resolution. To induce better waveforms, a rubber sheet was used as the pulse shaper and attached on the left end of the incident bar. The rubber sheets had an  $8.0 \text{ mm}$  diameter and were  $1.0 \text{ mm}$  thick.



**Figure 2.** (a) Experimental setup. (b) Schematic of steel specimen confinement chamber and wave propagation in the system.

### 2.2. Dynamic Stress Equilibrium

Based on the one-dimensional wave theory, the wave data were simplified, as recorded in detail by Gray [19].  $E$  was the Young’s modulus of the bar. By using the micro strain signal recorded by strain gauges of the incident bar and transmission bar, the incident stress history  $\sigma_i(t)$ , the reflected stress history  $\sigma_r(t)$ , the transmitted stress  $\sigma_t(t)$  could be recorded, combining the stress history of the incident and reflected waves, and comparing this against the stress history of the transmitted wave to assess dynamic stress equilibrium. Figure 3 shows the stress history during empty beating. It could be found that the dynamic stress curves of the incident wave and reflected wave were basically consistent with the transmitted wave after superposition, and the synchronicity indicated that dynamic stress equilibrium was achieved. It could be seen that the time taken for a complete loading pulse was approximately 475  $\mu$ s due to deformation of the rubber sheet.

Particle crushing must be accompanied by energy dissipation during impact. Based on the one-dimensional stress wave theory, the incident energy, reflected energy and transmitted energy were calculated using Formulas (1)–(3):

$$W_i = \frac{A}{\rho C} \int_0^t \sigma_i^2(t) dt \tag{1}$$

$$W_r = \frac{A}{\rho C} \int_0^t \sigma_r^2(t) dt \tag{2}$$

$$W_t = \frac{A}{\rho C} \int_0^t \sigma_t^2(t) dt \tag{3}$$

where  $t$  is time,  $A$  is the cross-sectional area of the steel bar,  $C$  is the wave propagation velocity within the steel bar,  $\rho$  is the density of the steel bar. Ignoring the energy lost at the interface between the specimen and the bar, the dissipated energy of the specimen can be expressed as Formula (4):

$$W_d = W_i - W_r - W_t \tag{4}$$

where  $W_d$  is the dissipated energy of the specimen during the impact process, mainly including crushing energy, friction energy, acoustic energy, thermal energy, radiation energy and other forms of dissipated energy.

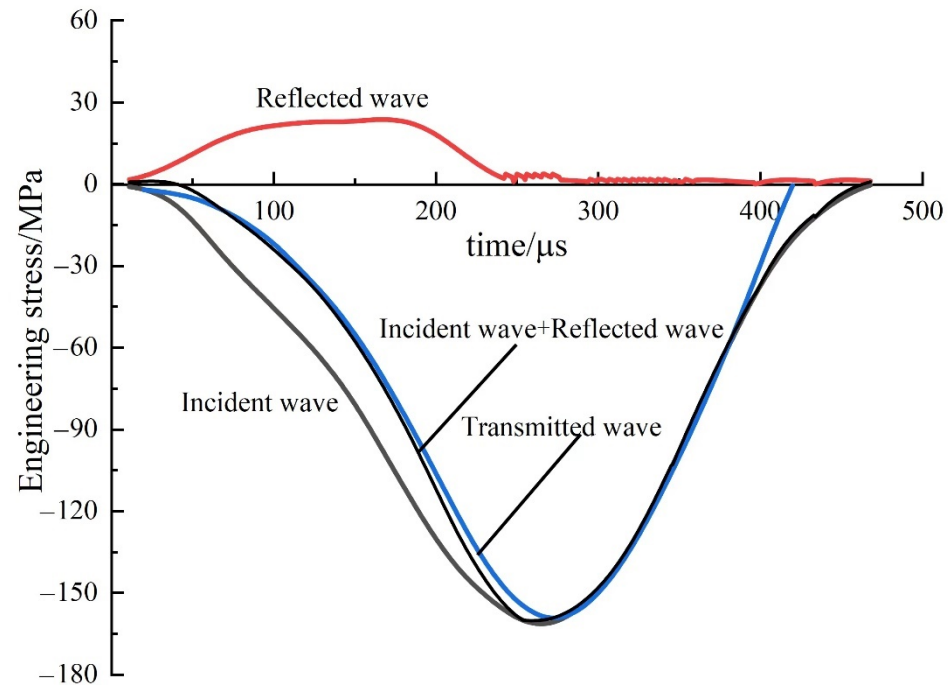


**Figure 3.** Typical response signals of incident, reflected and transmitted waves.

### 2.3. Specimen Preparation and Test Process

The test material was quartz sand and Kaolin clay. Quartz sand with a single mineral composition was a kind of granular material often used in the study of stress wave propagation in filled rock joints. Kaolin clay was commonly found in natural rock discontinuities. At the same time, it had good water absorption, and did not expand after water absorption. In the preparation of partially saturated specimens, it could be used as a water retaining agent to make the water distribution in partially saturated specimens more uniform.

The quartz sand was Fujian standard quartz sand and the major particle size was between 0.5 mm and 1 mm. The granule sizes of 0.5–0.8 mm accounted for about 70%, and 0.8–1.0 mm accounted for about 30%. The standard quartz sand oven dried at 105 °C. The initial dry density and voidage of quartz sand was 1.567 g/cm<sup>3</sup> and 41%. The clay was selected from Lingshou County washed Kaolin, which is a kind of clay widely existing in nature. The initial dry density and particle size of clay was 1.59 g/cm<sup>3</sup> and 100–200 mesh. The particle size distribution curves of sand and kaolin has been shown in Figure 4.

Each test confined the specimen in a 6 mm thick chamber. The gas chamber pressure constant was set to 0.2 MPa. There were 10 working conditions in the test, two parallel tests were carried out in each group of working conditions, and a total of 20 tests were conducted, with test numbers from T-1 to T-20 in sequence. T-1 to T-10 tests were conducted to investigate the influence of clay content on the propagation characteristics of the stress wave in artificial filled joints. The weight fractions of clay were 0%, 30%, 50%, 70% and 100%, respectively, and the corresponding dry densities were 1.569 g/cm<sup>3</sup>, 1.575 g/cm<sup>3</sup>, 1.578 g/cm<sup>3</sup>, 1.582 g/cm<sup>3</sup> and 1.590 g/cm<sup>3</sup>, respectively. The quartz sand and clay were uniformly mixed according to the mass ratio, and filled into the sleeve according to the fixed mass, which were filled with 18.45 g, 18.50 g, 18.54 g, 18.60 g and 18.68 g, respectively. T-3, T-4, T-11 to T-18 tests were conducted to investigate the influence of moisture content on the propagation characteristics of stress wave in artificial filled joints. Since the water in quartz sand mostly existed in the form of free water, it would sink into the bottom of the specimen because of the action of gravity during the test. Referring to the test method



of Huang et al. [20], clay was used as the water retention agent. Specimens with different saturation were prepared by adding a certain amount of water into sand–clay mixtures with 30% clay weight fraction. It was found that the specimen could basically approach a complete saturation state when 18.50 g sand–clay mixtures mixed with 4 g water. Therefore, 0 g, 1 g, 2 g and 3 g water were added to 18.50 g sand–clay mixtures, respectively, and the corresponding saturation  $S_r$  was 0%, 25%, 50% and 75%, respectively. When preparing saturated specimens, putting 18.50 g dry sand–clay mixtures into the sleeve, then putting sleeve into the vacuum saturation device, adding water until completely submerged. Opening the vacuum pump to pump the saturation device to vacuum, soaking for 10 min, then taking it out, so that the mixtures in the sleeve was saturated, then completing the impact test within 2 min. In the T-19 and T-20 group tests, the saturated quartz sand specimens were made by the above method as a comparative test.

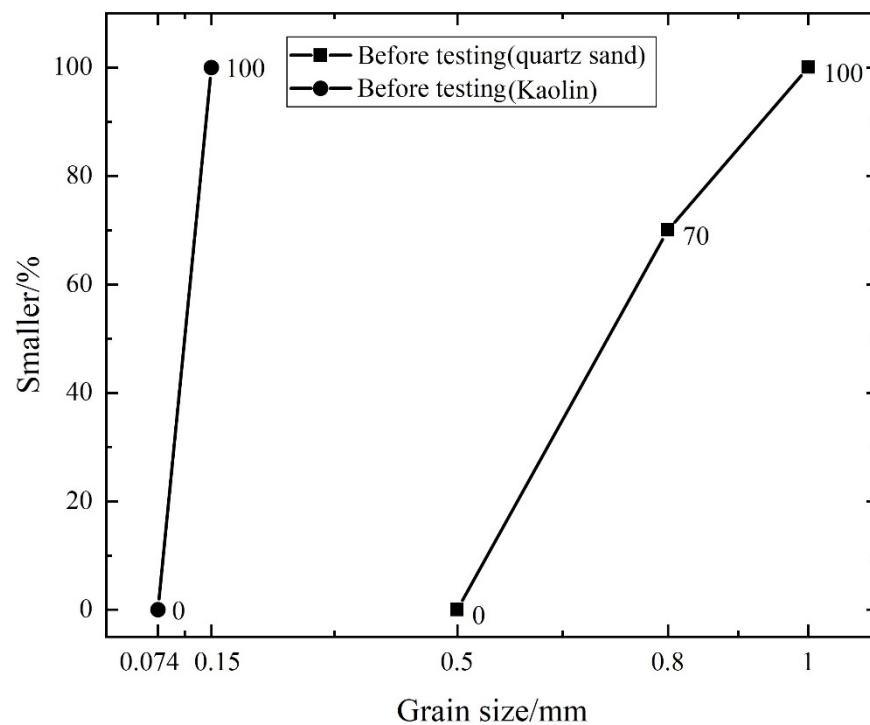


**Figure 4.** Particle size distribution curves of quartz sand and Kaolin before impact.

### 3. Results

The transmission coefficient based on peak stress was an important index to judge stress wave attenuation in rock joints. The wave transmission coefficient was defined as the ratio of the amplitude of the transmitted wave to that of the incident wave [21]; that is:

$$T = \frac{\sigma_{tmax}}{\sigma_{imax}} = \frac{\varepsilon_{tmax}}{\varepsilon_{imax}} \quad (5)$$

where  $T$  is the wave transmission coefficient,  $\sigma_{imax}$  and  $\sigma_{tmax}$  are the peak stresses of the incident wave and the transmitted wave,  $\varepsilon_{imax}$  and  $\varepsilon_{tmax}$  are the strains corresponding to the peak stresses of the incident wave and the transmitted wave.

The wave transmission coefficient  $T$  defined based on the peak stress of the incident wave and the transmitted wave represents the wave attenuation capacity of a specimen but not the infill materials, which are greatly affected by the thickness of the specimen. To describe the stress attenuation ability of granular material quantitatively, a dimensionless

modified attenuation coefficient  $k$  was proposed by removing the relative impedance of the bar to the specimen and considering the effects of the size of the specimen [22], as follows:

$$k = -\frac{D}{L_s} \ln(T) \quad (6)$$

where  $L_s$  is the length of the specimens,  $D$  is the diameter of the specimen, and  $T$  is the wave transmission coefficient.

The main results of the test are given in Table 1.

**Table 1.** The main results of the test.

Test Number	Clay Weight Fraction	Saturation $S_r$	Incident Wave Amplitude/MPa	Transmitted Wave Amplitude/MPa	Attenuation Coefficient $k$	Incident Energy $W_i$ /J	Reflected Energy $W_r$ /J	Transmitted Energy $W_t$ /J	Dissipated Energy $W_d$ /J
T-1	0%	0%	155.2	28.7	14.07	165.7	120.2	4.7	40.8
T-2	0%	0%	149.3	31.6	12.94	158.8	98.2	6.8	53.8
T-3	30%	0%	150.2	32.5	12.76	168.9	138.5	6.1	24.3
T-4	30%	0%	153.8	33.6	12.68	167.0	126.9	6.4	33.7
T-5	50%	0%	164.3	55.1	9.10	169.4	134.2	14.0	21.2
T-6	50%	0%	167.9	48.8	10.30	170.5	113.8	18.6	38.1
T-7	70%	0%	154.8	29.4	13.84	160.9	127.9	4.6	28.4
T-8	70%	0%	164.3	30.1	14.14	168.5	130.1	5.1	33.3
T-9	100%	0%	164.8	13.1	21.10	169.6	139.7	0.7	29.2
T-10	100%	0%	159.4	10.4	22.75	169.0	139.4	0.8	28.8
T-11	30%	25%	162.9	15.5	19.60	163.2	140.8	0.8	21.6
T-12	30%	25%	165.9	16.0	19.49	163.1	135.5	1.9	25.7
T-13	30%	50%	162.7	73.0	6.68	159.0	92.1	24.2	42.7
T-14	30%	50%	163.5	72.8	6.74	152.1	86.0	20.4	45.7
T-15	30%	75%	156.9	90.1	4.62	165.6	69.7	41.1	54.8
T-16	30%	75%	167.7	99.6	4.34	153.8	51.8	49.1	52.9
T-17	30%	100%	169.2	110.7	3.54	159.2	46.5	68.3	44.4
T-18	30%	100%	168.0	117.0	3.01	155.2	42.6	64.0	48.6
T-19	0%	100%	157.3	118.8	2.34	165.8	37.1	95.1	33.6
T-20	0%	100%	151.5	102.2	3.28	159.9	35.4	90.2	34.3

According to Table 1, when the gas pressure was 0.20 MPa, the amplitudes of the incident waves ranged from 149.3 MPa to 169.2 MPa. For the same gas pressure, the incident wave amplitude was similar and the test conditions were basically the same. Therefore, the tests had good repeatability and high reliability.

The incident wave and transmission wave of artificial filled joints with different Kaolin weight fractions are plotted in Figure 5a. Under the condition of similar incident wave amplitude, the amplitude of the transmitted waves of 50% Kaolin weight fractions is much higher than that of transmitted waves corresponding to other working conditions. When the gas pressure is 0.20 MPa, the amplitudes of the transmitted waves of the 50% Kaolin weight fractions ranged from 48.8 MPa to 55.1 MPa. With the increase of Kaolin weight fractions, the amplitude of transmitted wave increases first and then decreases. When the weight fraction of Kaolin was 100%, the amplitude of transmitted wave is the smallest, only ranging from 10.4 MPa to 13.1 MPa, which is decreased by about 77% compared with the highest amplitude of transmitted wave.

According to Table 1, as shown in Figure 5b, with the increase in the weight fractions of Kaolin, the average attenuation coefficient  $k$  decreases first and then increases. When the weight fraction of Kaolin is 30%, the average attenuation coefficient is close to that of quartz sand. When the weight fraction of Kaolin was 50%, the minimum attenuation coefficient was 9.70. When the weight fraction of Kaolin was 100%, the maximum attenuation coefficient was 21.92. It could be considered that under the impact of high amplitude

incident wave, when the weight fraction of Kaolin was 50%, the spaces between quartz sand would be filled by Kaolin during compaction. The overall porosity of the artificial filled joint was the lowest, the overall stiffness was the highest, and the wave attenuation degree was the smallest.

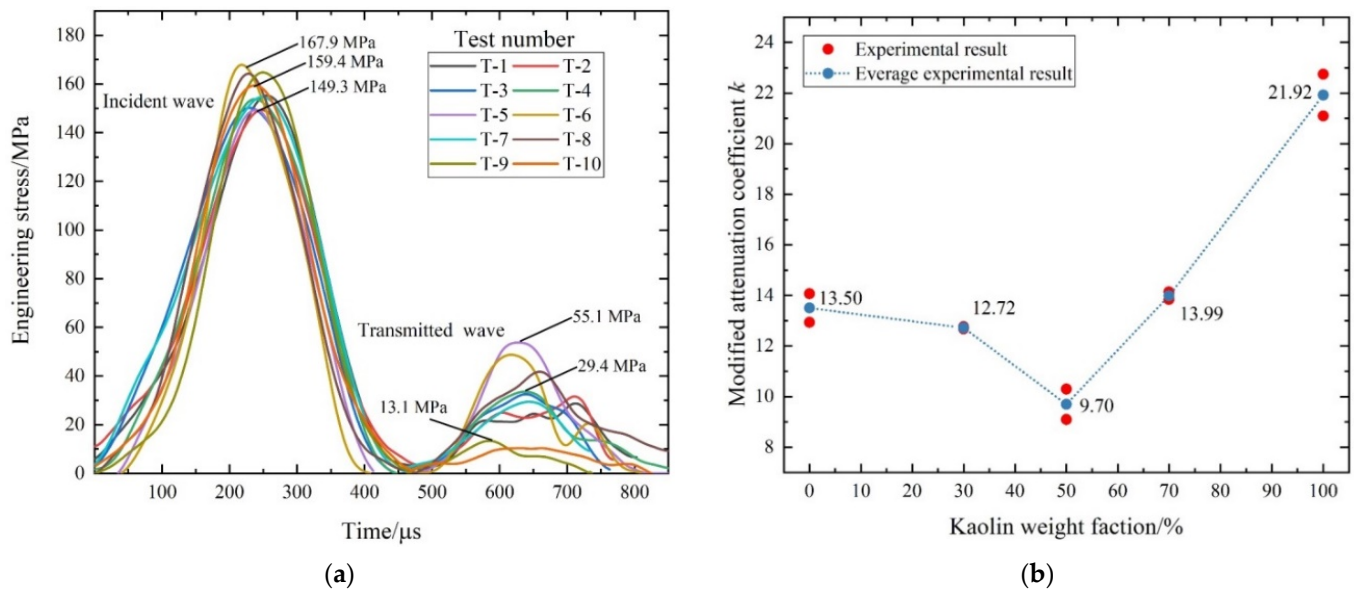


**Figure 5.** The artificial filled joints with different Kaolin weight fractions correspond to: (a) incident wave and transmission wave; (b) Attenuation coefficient curve.

The incident wave and transmission wave of artificial filled joints with different saturation  $S_r$  are plotted in Figure 6a. With the increase of saturation, the amplitude of transmitted wave decreased first and then increased. When the saturation of specimen was 25%, the amplitude of the transmitted wave was the smallest and only ranged from 15.5 MPa to 16.0 MPa; when the saturation of the specimen was 100%, the amplitude of the transmitted wave was the largest and ranged from 110.7 MPa to 117.0 MPa. This result was consistent with that reported in reference [23]. When the saturation was low, the spaces between the particle skeletons were not filled with water, and deformation could still occur. Meanwhile, the presence of water reduced the frictional force between particles and made it easier to slide and rearrange. As the saturation increased further, the spaces between the skeletons were gradually filled with water. Because the pore water was incompressible, it was more and more difficult for particles to move into the space, and the pore water bore more loading, thereby increasing the overall stiffness. When the saturation reached 75%, the amplitude of the transmitted wave was close to that of the saturated specimen, ranging from 90.1 MPa to 99.6 MPa. This phenomenon reflected the porous gas of partially saturated granular materials was discharged during high-amplitude impact, gradually changing from the initial three-phase system to a two-phase system, and the pore water began to support the external load with the solid skeleton together.

As shown in Figure 6b, when the degree of saturation was 25%, the maximum average attenuation coefficient was 19.55 and when the degree of saturation was 100%, the minimum average attenuation coefficient was 3.30. The average attenuation coefficient of saturated quartz sand specimen as the control group was 2.81, which was similar to that of quartz sand–clay mixtures. It could be considered that the transmission and attenuation of the stress wave were only related to water, but not related to the particle skeleton under the saturated condition. After the water filled the space completely, the specimen could hardly deform. However, the existence of Kaolin made a certain amount of small bubbles around the particle skeleton not able to be discharged, which may lead to a certain attenuation of the stress wave.



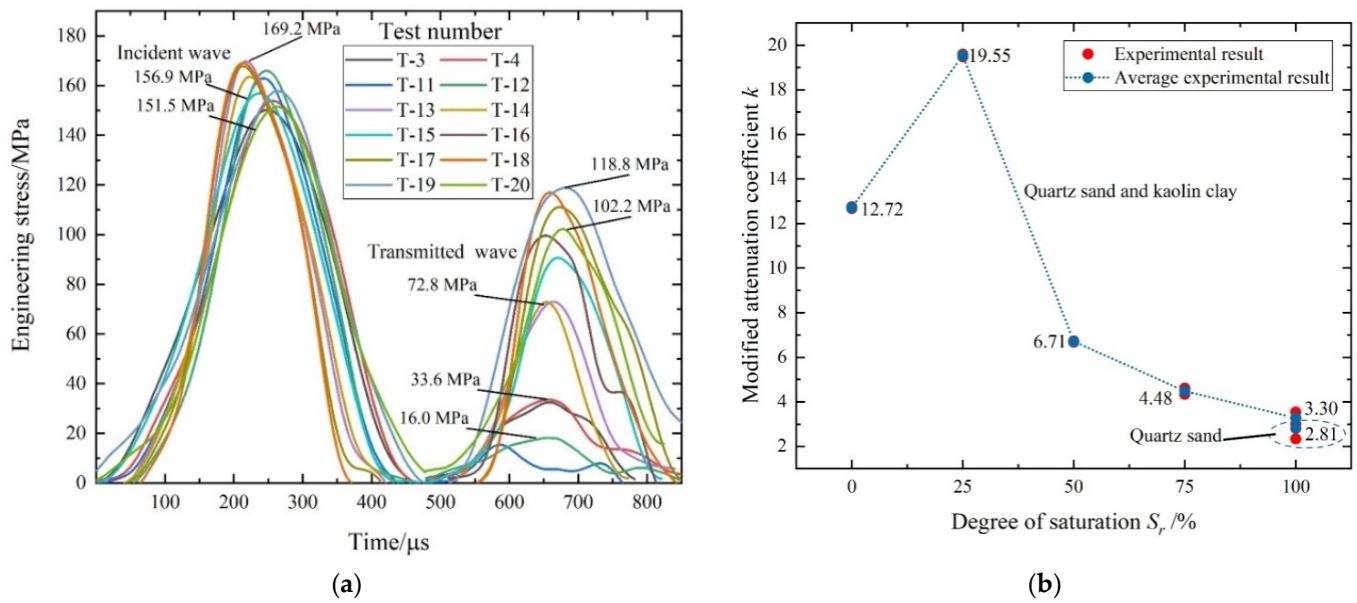


**Figure 6.** The artificial filled joints with different saturation  $S_r$  correspond to: (a) incident wave and transmission wave; (b) Attenuation coefficient curve.

#### 4. Discussion

##### 4.1. Particle Crushing Behavior

Particles experienced compaction and crushing with high-amplitude stress waves propagation across a filled fracture. The process of particle crushing was not only related to the dynamic compression process of the whole specimen, but also determined the amount of energy dissipation when the seismic wave transmission across the filling material. By analyzing the degree of the particle crushing, the deformation mechanism in the whole process could be obtained indirectly [24]. Previous works have found that particle crushing was affected by many factors, such as initial void, particle size, particle grading composition, strain rate, loading condition, constraint condition, etc. [25,26]. However, when the specimen was saturated, the crushing of particles could not be fully reflected from the gradation curve because the water was incompressible, so it needs further discussion. The test work results were quantified by the relative breakage potential  $B$  which was given by Hardin [27]:

$$B = \frac{B_t}{B_p} \tag{7}$$

where  $B_p$  is the breakage potential, which was defined as the area between the lower bound of the 0.074 mm sieve opening and the original size distribution curve, and  $B_t$  is the total breakage, which was defined as the area between the original and the final size distribution curves.

As shown in Figure 7a, as the weight fraction of Kaolin decreased from 70% to 0%, a considerable number of particles were crushed into smaller particles. The dependence of filler deformation on the amplitude of the stress wave could be divided into three stages: initial compaction stage, crushing stage, and compaction and crushing stage. When the gas pressure was set to 0.20 MPa, the particle skeleton of the pure quartz sand specimen mainly in the compaction and crushing stage, the particles were seriously crushing, and the relative breakage potential  $B$  was the largest, which was 0.29. With the increase of clay content, the volume of clay was compressed under high amplitude impact. Because the clay could not be further crushed, the clay filled the space between the skeletons and reduced the particle deformation space. The stiffness of the artificial joint was increased, and the wave attenuation was reduced. When the Kaolin weight fraction was 30%, after the clay was compressed, the quartz sand skeleton still had deformation space, the relative breakage potential  $B$  decreased less, and the wave attenuation was larger. When the weight fraction

of Kaolin was 50%, the void of the specimen was completely filled by the compressed clay during impact, and the rigidity of the specimen reached the maximum, and the wave attenuation was small. When the weight fraction of Kaolin further increased, the particle skeleton was no longer the force subject, and waves were absorbed and attenuated during the compression process of clay. With the increase of clay content, the wave attenuation performance decreased first and then increased, the relative breakage potential  $B$  decreased continuously, and the same trend did not appear.

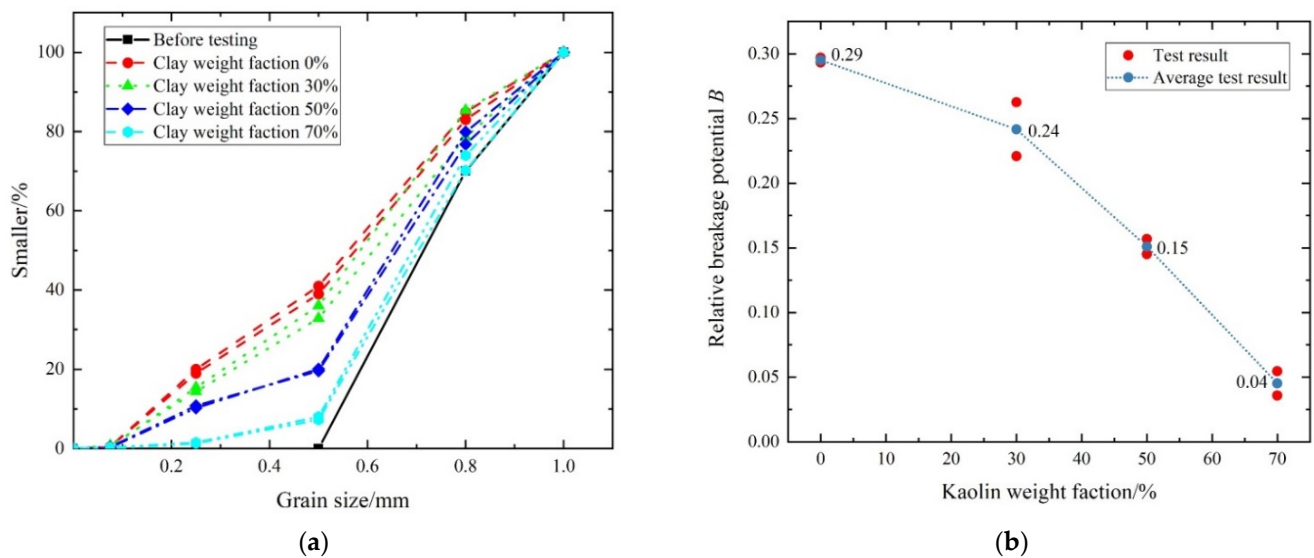


**Figure 7.** (a) Particle size distribution curves of specimens with different Kaolin weight fractions after impact. (b) Variation diagram of average relative breakage potential.

According to the test data of T-3, T-4, T-11 to T-20 groups in Figure 8, it could be found that when the Kaolin weight fraction was 30%, with the increase of saturation, the relative breakage potential  $B$  decreased first, then increased and then decreased. As the saturation increased from 0% to 25%, the relative breakage potential  $B$  decreased from 0.24 to 0.16. Compared with the saturation of 50%, the relative breakage potential  $B$  was 0.19. Analyzing the reason was that when the saturation was 25%, under the high amplitude impact, the existence of water between particles led to the decrease of friction between particles. First, the particles slid relatively to the space compaction and then the particles crushed. When the saturation was low, there was more relative sliding and less particle crushing, and as the saturation increased to 50%, because the water was incompressible, the further increase in saturation caused the pore water to take away more load from the skeleton, making it difficult for the particles to move into the void, thus increasing the overall stiffness. Under the high amplitude impact, the particle skeleton cannot slide and was crushed, and the relative breakage potential  $B$  had a certain increase. With the further increase of saturation, the air in the pore was completely discharged when the stress was lower and the saturated state was reached during the impact process. The free water was completely filled in the void; since the water was incompressible and mainly provides hydrostatic pressure, the specimen could not be crushed. The parameter  $B$  of relative crushing probability decreases continuously and reaches the minimum when saturated.

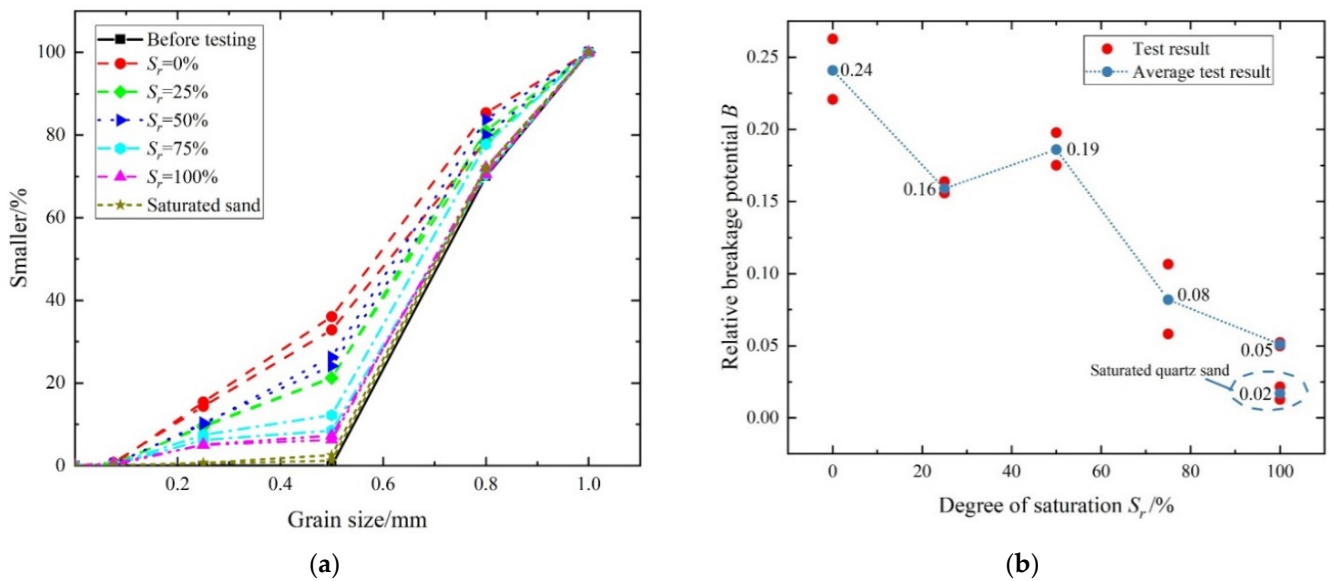


**Figure 8.** (a) Particle size distribution curves of specimens with different saturations after impact. (b) Variation diagram of average relative breakage potential.

Compared with the saturated pure quartz sand and quartz sand–clay mixtures, the presence of clay may make the existence of small bubbles unable to be discharged. During the impact process, the irregular corner friction of quartz sand would be broke, resulting in the increase of particles within the range of 0.075–0.25 mm.

#### 4.2. Energy Distribution

By analyzing the energy distribution, the particle crushing and particle friction in the further test could be judged. It could be found from Table 1 that when the gas pressure was set to 0.2 MPa, the incident energy ranged from 152.1 J to 170.5 J. Under the same incident energy condition, friction energy consumption between particles increased with the increase of relative slip and dissipated energy increased with the increase of serious particle crushing. These two factors make the specimens have greater absorption energy.

According to the test data of groups T-1 to T-10, as shown in Figure 9a, it could be found that under the condition of similar incident energy, there was no obvious change rule of reflected energy under various working conditions, but numerically the proportion of reflected energy to the total incident energy was large, with an average proportion of 67.2–82.4%, and only a small part of the energy could transmit. With the increase of the Kaolin weight fraction, the average transmitted energy proportion increased from 3.6% to 9.6% when the Kaolin weight fraction was 50%, then the proportion of transmitted energy decreased gradually. When the Kaolin weight fraction was 100%, the transmitted energy was the smallest, which was 0.4%. By analyzing the dissipated energy, it was mainly related to particle crushing and friction. Through the change curve of the relative breakage potential  $B$  in Figure 7b, it could be found that the change rule of the average dissipated energy ratio was the same as that of Figure 7b. With the increase of the Kaolin weight fraction, the average dissipated energy ratio decreased continuously, and the relative breakage potential  $B$  also decreased continuously, showing that the particle crushing decreased. Comparing the wave attenuation coefficient, particle crushing and energy distribution, it could be found that when the weight fraction of Kaolin was 50%, the overall wave attenuation ability was the worst and the proportion of transmitted energy was the largest. Compared with Wu et al. [13], it was found that when the weight fraction of Kaolin was 30%, the wave attenuation performance of the specimen was the worst, the Kaolin selected by him was crushed to below 0.25 mm, and the mass density of Kaolin was 1.631 g/cm<sup>3</sup>. Before the test, he mixed the sand with water uniformly and dried it, then impacted it at low strain rate. In this paper, the dry loose clay was selected for the test, with a larger space. It was a high-

amplitude impact in this paper. Firstly, the clay component was compressed to reach the closest state, and then the quartz sand particle skeleton was compressed; when the Kaolin weight fraction was 30%, there were still a lot of space after compression. When the Kaolin weight fraction was 50%, the specimen reached the closest state after compression, the space was the smallest, the specimen stiffness was the largest, the corresponding transmitted energy was the largest, and the wave-absorbing performance was the weakest.

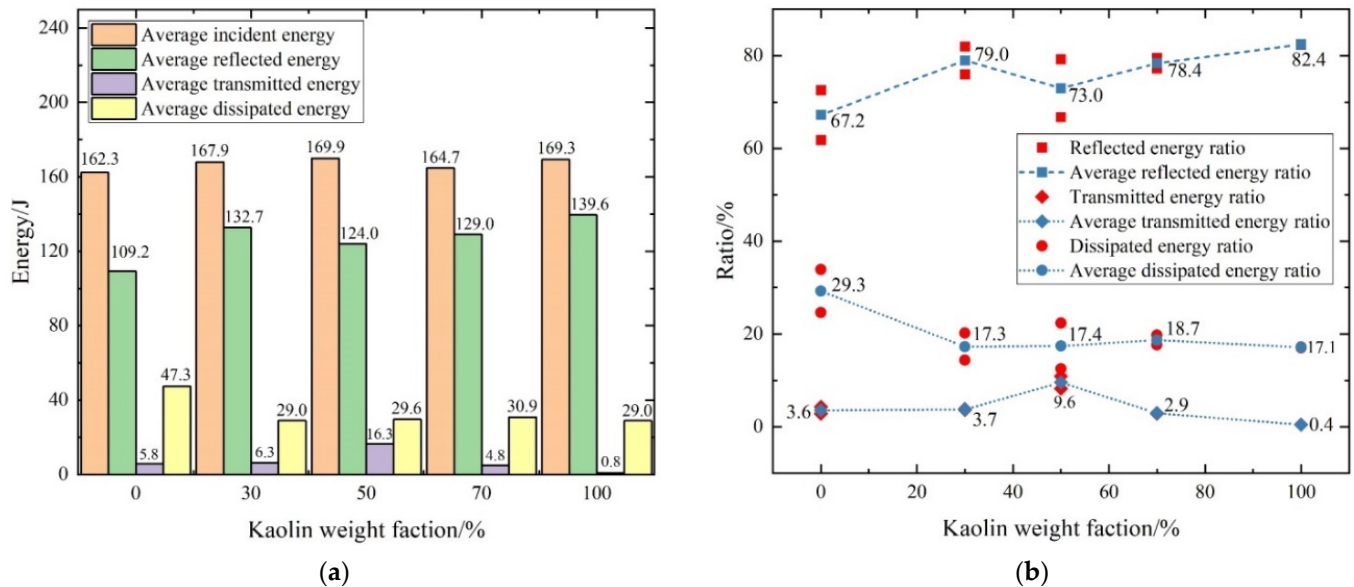


**Figure 9.** (a) Energy distribution histogram of specimens with different Kaolin weight fractions after impact. (b) Ratio curve of each part energy to incident energy.

According to the test data of groups T-3, T-4, T-11 to T-20, as shown in Figure 10, it could be found that as the saturation increased, the ratio of the three kinds of energy to the total incident energy showed a different trend from that in Figure 9b. With the increase of saturation, the reflected energy increased first. When the saturation was 25%, the reflected energy was the largest, then decreased with the increase of saturation. The dissipated energy and transmitted energy decreased first and then increased continuously. For the dissipated energy, it can be found that when the saturation was 25%, the relative breakage potential  $B$  was 0.159, which was lower than that of the saturation of 0% and 50%, but the dissipated energy was similar to that of the saturation of 0%. This part of the energy may be mainly dissipated by friction sliding. With the further increase of saturation, the dissipated energy increased further, but the relative breakage potential  $B$  decreased continuously. At this time, the energy was mainly absorbed by water and the water was basically incompressible. The particles were mainly subjected to uniform hydrostatic pressure in all directions, and the particles could not be broken. The characteristics of the transmitted energy showed the most soft characteristics when the saturation was 25%, and the transmitted energy account for the smallest proportion, which was similar to the previous experimental results.

Meanwhile, compared with the energy ratio of T-19 and T-20 saturated quartz sand, the saturated sand has less reflected energy, greater transmitted energy and dissipated energy, more energy transmitted, and the particles were crushed less. As shown in Figure 7a, it can be found that there were basically no particles crushing and more energy was absorbed by water. The reason for this phenomenon is that clay can absorb water. Because of the decrease in the content of free water, the water-bearing value is reduced. In this way, the pellet skeleton can take more load.



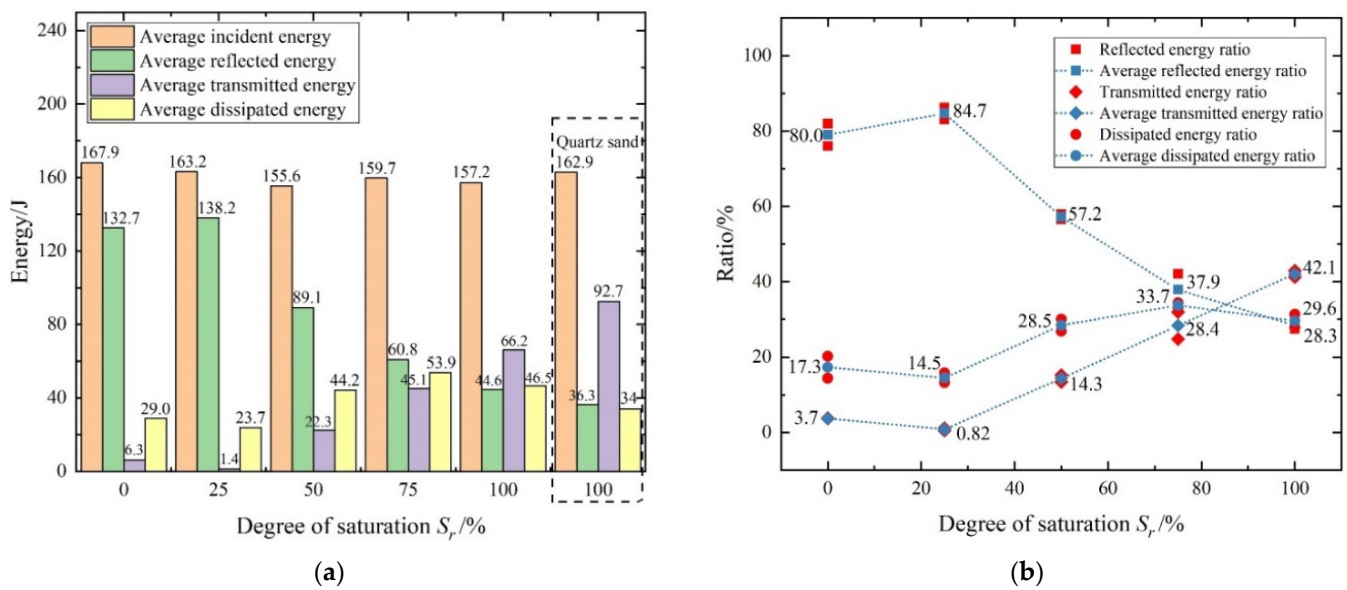


**Figure 10.** (a) Energy distribution histogram of specimens with different saturations after impact. (b) Ratio curve of each part energy to incident energy.

## 5. Conclusions

In order to explore the influence of clay content and moisture content on the wave attenuation characteristics of filling fissures in surrounding rock under a high-amplitude seismic wave, the split Hopkinson pressure bar (SHPB) test technique was used to conduct high-amplitude impact tests on artificial filled joints composed of sand–clay mixtures with different clay mass fractions and saturations. The conclusions are as follows:

1. With the increase of the clay weight fraction, the wave attenuation coefficient decreased first and then increased. When the weight fraction of Kaolin was 50%, the attenuation coefficient was 9.70, which is the minimum among the tested working conditions. As the saturation increased, the wave attenuation coefficient reached a maximum when the saturation was 25%, and then began to decrease as the saturation increased.
2. With the increase of the clay weight fraction, the relative breakage potential  $B$  decreased continuously, and the proportion of dissipation energy to total incident energy also decreased. The variation trend of the transmitted energy ratio was the same as that of the wave attenuation coefficient. When the clay mass fraction was 25%, the proportion of transmitted energy to total incident energy reached the maximum.
3. With the increase of saturation, when the saturation was 25%, the friction between particles decreased due to the lubrication of water, and the corresponding transmitted energy was the lowest. When the saturation reached 100%, the wave attenuation coefficient of sand–clay mixtures was the smallest, and the proportion of transmitted energy reached 42.1%. Compared with quartz sand and sand–clay mixture, the wave attenuation coefficient was similar. It could be considered that the wave transmission characteristics was independent of the filling materials under saturated conditions. However, due to the presence of bound water in clay, the particles crushed due to the presence of tiny bubbles during impact.

**Author Contributions:** S.L.: Investigation, Methodology, Formal Analysis, Writing—Original Draft; Z.X.: Methodology, Supervision, Validation, Writing—Review & Editing; P.F.: Conceptualization, Funding Acquisition, Resources, Project Administration, Validation, Writing—Review & Editing; K.X.: Data Curation, Investigation. All authors have read and agreed to the published version of the manuscript.



**Funding:** This research was funded by the National Natural Science Foundation of China (NSFC) (grant number 51979280) and the National Natural Science Foundation of China (NSFC) (grant number 52009138).

**Data Availability Statement:** Not applicable.

**Conflicts of Interest:** The authors declare no conflict of interest.

## References

1. Liu, X.; Xu, H.; Fan, P.; Geng, H.; Mo, J.; Wang, D. Experimental study on the stress wave attenuation effect of filled cracks in rocks under confining pressure. *Rock Soil Mech.* **2021**, *42*, 2099–2108+2119.
2. Wang, M.Y.; Guo, S.B.; Zhao, Y.T.; Yan, H.J.; Zhao, Y. Progression of liquefaction investigation for saturated sand soil under dynamic loading. *J. F PLA Univ. Sci. Technol.* **2002**, *1*, 13–18.
3. Wang, M.Y.; Qian, Q.H. Attenuation law of explosive wave propagation in cracks. *Chin. J. Geotech. Eng.* **1995**, *17*, 42–46.
4. Bragov, A.M.; Lomunov, A.K.; Sergeichev, I.V.; Tsembelis, K.; Proud, W.G. Determination of physico-mechanical properties of soft soils from medium to high strain rates. *Int. J. Impact Eng.* **2008**, *35*, 967–976. [[CrossRef](#)]
5. Chen, H.; Zhang, C.; Wei, J.; Li, M.; Wang, Y. A modified method for estimating the stress state of granular materials in the passive confined pressure SHPB tests. *Int. J. Impact Eng.* **2022**, *160*, 104063. [[CrossRef](#)]
6. Wang, S.; Shen, L.; Nguyen, G.D.; Maggi, F.; El-Zein, A.; Zheng, Y. An empirical approach for the quantification of uniaxial compressive stress-strain of partially saturated granular media under high strain rates. *Soil Dyn. Earthq. Eng.* **2019**, *120*, 245–256. [[CrossRef](#)]
7. Luo, H.; Lu, H.; Cooper, W.L.; Komanduri, R. Effect of mass density on the compressive behavior of dry sand under confinement at high strain rates. *Exp. Mech.* **2011**, *1*, 1499–1510. [[CrossRef](#)]
8. Luo, H.; Cooper, W.L.; Lu, H. Effect of moisture on the compressive behavior of dense Eglin sand under confinement at high strain rates. *Int. J. Impact Eng.* **2014**, *65*, 40–55. [[CrossRef](#)]
9. Barr, A.D.; Clarke, S.D.; Tyas, A.; Warren, J.A. Effect of moisture content on high strain rate compressibility and particle breakage in loose sand. *Exp. Mech.* **2018**, *58*, 1331–1334. [[CrossRef](#)]
10. De Cola, F.; Pellegrino, A.; Glößner, C.; Penumadu, D.; Petrinic, N. Effect of particle morphology, compaction, and confinement on the high strain rate behavior of sand. *Exp. Mech.* **2018**, *58*, 223–242. [[CrossRef](#)]
11. Meyers, M.A. *Dynamic Behavior of Materials*; John Wiley and Sons: New York, NY, USA, 1994; pp. 179–201.
12. Lak, M.; Marji, M.F.; Bafghi, A.Y.; Abdollahipour, A. Analytical and numerical modeling of rock blasting operations using a two-dimensional elasto-dynamic Green's function. *Int. J. Rock Mech. Min. Sci.* **2019**, *114*, 208–217. [[CrossRef](#)]
13. Lak, M.; Marji, M.F.; Bafghi, A.Y.; Abdollahipour, A. A Coupled Finite Difference-Boundary Element Method for modeling the propagation of explosion-induced radial cracks around a wellbore. *J. Nat. Gas Sci. Eng.* **2019**, *64*, 41–51. [[CrossRef](#)]
14. Li, J.C.; Wu, W.; Li, H.B.; Zhu, J.B.; Zhao, J. A thin-layer interface model for wave propagation through filled rock joints. *J. Appl. Geophys.* **2013**, *91*, 31–38. [[CrossRef](#)]
15. Li, J.C.; Ma, G.W.; Huang, X. Analysis of Wave Propagation Through a Filled Rock Joint. *Rock Mech. Rock Eng.* **2010**, *43*, 789–798. [[CrossRef](#)]
16. Wang, H.; Chai, S.B.; Yu, L.Y.; Jin, Y.L.; Zhou, T.L. P-wave propagation across a viscous-elastic rock mass with a structural plane. *Chin. J. Rock Mech. Eng.* **2020**, *39* (Suppl. S1), 2763–2770.
17. Luo, H.; Hu, Z.; Xu, T.; Guo, L.; Lu, H. High-strain rate compressive behavior of a “natural soil” under uniaxial strain state. In *Dynamic Behavior of Materials*; Kimberley, J., Lamberson, L., Mates, S., Eds.; Springer: Cham, Switzerland, 2018; Volume 1, pp. 87–92. [[CrossRef](#)]
18. Wu, W.; Li, J.C.; Zhao, J. Role of filling materials in a P-wave interaction with a rock fracture. *Eng. Geol.* **2014**, *172*, 77–84. [[CrossRef](#)]
19. Gray, G. Classic Split-Hopkinson Pressure Bar Testing. In *Mechanical Testing and Evaluation, Metals Handbook*; American Society for Metals: Material Park, OH, USA, 2000; Volume 8, pp. 462–476.
20. Huang, X.; Qi, S.; Yao, W.; Xia, K. Effect of filling humidity on the propagation of high-amplitude stress waves through an artificial joint. *Geotech. Test. J.* **2019**, *42*, 30–42. [[CrossRef](#)]
21. Li, J.C.; Li, N.N.; Li, H.B.; Zhao, J. An SHPB test study on wave propagation across rock masses with different contact area ratios of joint. *Int. J. Impact Eng.* **2017**, *105*, 109–116. [[CrossRef](#)]
22. Lv, Y.R.; Ng, C.W.W.; Wang, Y.A. Evaluation of wave dissipation in sand under impact loading. *J. Geotech. Geoenviron. Eng.* **2019**, *145*, 06019007. [[CrossRef](#)]
23. Martin, B.E.; Chen, W.; Song, B.; Akers, S.A. Moisture effects on the high strain-rate behavior of sand. *Mech. Mater.* **2009**, *41*, 786–798. [[CrossRef](#)]
24. Wang, J.; Fan, P.; Wang, M.; Dong, L.; Ma, L.; Gao, L. Experimental study of one-dimensional compression creep in crushed dry coral sand. *Can. Geotech. J.* **2020**, *57*, 1854–1869. [[CrossRef](#)]
25. Ma, L.; Li, Z.; Wang, M.; Wei, H.; Fan, P. Effects of size and loading rate on the mechanical properties of single coral particles. *Powder Technol.* **2018**, *342*, 961–971. [[CrossRef](#)]

26. Huang, J.; Xu, S.; Hu, S. Effects of grain size and gradation on the dynamic responses of quartz sands. *Int. J. Impact Eng.* **2013**, *59*, 1–10. [[CrossRef](#)]
27. Hardin, B.O. Crushing of soil particles. *J. Geotech. Eng. Div.* **1985**, *111*, 1177–1192. [[CrossRef](#)]